Inhomogeneity of block copolymers at the interface of an immiscible polymer blend

Ji Ho Ryu,[1] YongJoo Kim,[2] and Won Bo Lee[1,*]

[1]*School of Chemical and Biological Engineering, Institute of Chemical Processes, Seoul National University, Seoul 08826, Republic of Korea*

[2]*KAIST Institute for the Nanocentury, Korea Advanced Institute of Science and Technology, Daejeon 34141, Republic of Korea*

(Received 17 April 2017; published 18 April 2018)

We present the effects of structure and stiffness of block copolymers on the interfacial properties of an immiscible homopolymer blend. Diblock and two-arm grafted copolymers with variation in stiffness are modeled using coarse-grained molecular dynamics to compare the compatibilization efficiency, i.e., reduction of interfacial tension. Overall, grafted copolymers are located more compactly at the interface and show better compatibilization efficiency than diblock copolymers. In addition, an increase in the stiffness for one of the blocks of the diblock copolymers causes unusual inhomogeneous interfacial coverage due to bundle formation. However, an increase in the stiffness for one of blocks of the grafted copolymers prevents the bundle formation due to the branched chain. As a result, homogeneous interfacial coverage of homopolymer blends is realized with significant reduction of interfacial tension which makes grafted copolymer a better candidate for the compatibilizer of immiscible homopolymer blend.

DOI: 10.1103/PhysRevE.97.042502

I. INTRODUCTION

Polymer blends are generally used to tailor and provide superior properties that may not be obtained from single polymers. For example, blending the electron donor and acceptor polymers improves the energy conversion efficiency and carrier collection efficiency of organic photovoltaic cells [1–5], and blends of polystyrene and Acrylonitrile-Butadiene-Styrene show enhanced Young's modulus and tensile strength [6]. Most homopolymer blends are incompatible due to low mixing entropy originating from the high molecular weights of the polymers resulting in macrophase separation of homopolymers [7–11]. Furthermore, minimizing unfavorable interaction energy from the interface of macrophase separated homopolymers results in poor mechanical properties due to weak interfacial adhesion [1]. The copolymers, which have affinity to both homopolymers, is used to stabilize the homopolymer blends by regulating the interfacial properties [1,7,12–17]. The effects of interplay between homopolymer blends and diblock copolymers as a compatibilizer on the thermodynamic and local structural properties at the interface have already been studied experimentally [13,18] and computationally [9,12,14–17,19]. Previous studies on the effect of copolymer structure on the interfacial properties of polymer blends have been conducted using the numerical self-consistent field theory [12,16,17,20–22], which can be accurate in the limit of infinite chain length. The recent experimental study on the compatibilization efficiency between diblock and grafted copolymers, which have relatively short finite chain length, in organic photovoltaic cells, showed that grafted copolymer is a better compatibilizer [1]. In addition, semiflexible copolymers which contain π-conjugated polymer blocks are widely used for regulating the interfacial properties of polymer blend systems in manufacturing organic thin-film transistor [23] and bulk heterojunction photovoltaic cells [1–3]. In this manner, systematic theoretical study of short copolymers as compatibilizer with various structures and stiffness of chain is required to elucidate the interfacial properties of homopolymer blends.

In this article, we investigated how the interfacial properties of polymer blends are affected by the structure and the subchain stiffness of the copolymer compatibilizer using coarse-grained molecular dynamics. For simulating the polymer blend as in the experimental study [1], two types [A and B beads from Figs. 1(a) and 1(b)] of comparatively short homopolymers ($N_{\mathrm{homo}} \leqslant 30$) were used to compose the blend, were N_{homo} is the number of beads in a homopolymer. The number density was set to $\rho = 0.85\sigma^{-3}$, which is the typical value for a polymer melt simulation [24–27], where ρ is the number density of system. Molecular dynamics simulation is used in this study to investigate the intermolecular correlations and the interfacial fluctuations [24,26,28]. In addition, to investigate the unusual behaviors of semiflexible copolymers near the interface [29–31], we focus on how the interfacial properties of a binary blend system changes with the subchain stiffness of copolymers.

II. SIMULATION METHODS

The Kremer–Grest bead-spring model is used to construct the coarse-grained polymer system [24–27,32,33]. The nonbonded interaction potential $U^{ij}_{\mathrm{WCA}}(r)$, $i,j = \{A,B\}$, between A bead and B bead is expressed as the truncated and purely repulsive Lennard–Jones potential, namely the Weeks–Chandler–Andersen (WCA) potential, [34] shown as follows:

$$U^{ij}_{\mathrm{WCA}}(r) = 4\varepsilon_{ij}[(\sigma_{ij}/r)^{12} - (\sigma_{ij}/r)^{6} + 1/4], \qquad (1)$$

where the cutoff radius is $r_c = 2^{1/6}\sigma$ with $U^{ij}_{\mathrm{WCA}}(r) = 0$ for $r > r_c$, and σ_{ij} and ε_{ij} are the parameters for the bead diameter

*wblee@snu.ac.kr

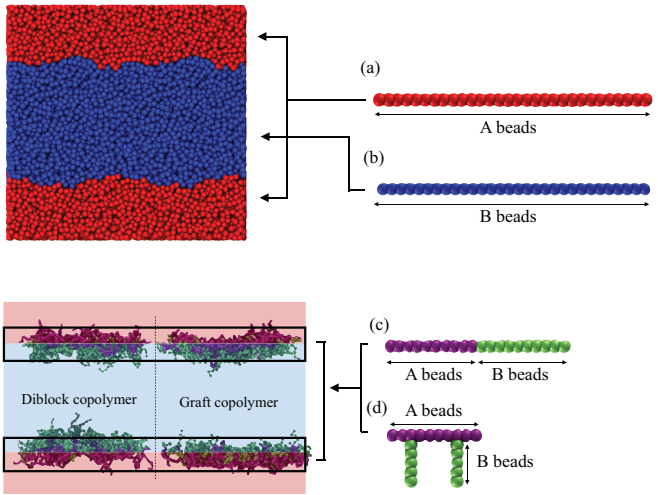

FIG. 1. The images of (a) A homopolymer, (b) B homopolymer, (c) diblock copolymer, and (d) two-arm grafted copolymer. A/B homopolymers are modeled by connecting 30 A beads and 30 B beads, respectively. The diblock copolymer is described by linearly connected 10 A beads and 10 B beads and the grafted copolymer is modeled with two B blocks, which are composed of 5 B beads, grafted on the third and eighth beads along the backbone chain consisting of 10 beads of type A.

and the energy between the ith bead and the jth bead; $i, j = \{A, B\}$. The neighboring beads are connected by the bonding potential, i.e., the finitely extensible nonlinear elastic (FENE) potential $U_{\mathrm{FENE}}(r)$.

$$U_{\mathrm{FENE}}(r) = -0.5 k_b R_0^2 \ln[1 - (r/R_0)^2], \tag{2}$$

with $k_b = 30\varepsilon\sigma^{-2}$ and $R_0 = 1.5\sigma$ to make the chain crossing energetically infeasible and provide equilibrium length $\langle l \rangle \sim 0.97\sigma$. Two types of copolymers, diblock and two-arm grafted copolymers, are used to compare the compatibilization efficiency in the immiscible homopolymer blends, which is the amount of interfacial tension reduction. In this particular study, we only considered copolymers with symmetric volume fraction of A and B. The diblock copolymer is described by linearly connecting 10 A beads and 10 B beads as shown in Fig. 1(c). Two-arm grafted copolymer is modeled by grafting two branch chains, which are composed of 5 beads of type B, connected on the third and eighth beads of the linearly connected backbone chain consisting of 10 A beads as shown in Fig. 1(d). In addition to the elastic potential between neighboring beads, we implemented additional harmonic angle potential $U_{\mathrm{Angle}}(\theta)$ to the stiff subchain block consisting of A beads (SubA) defined as

$$U_{\mathrm{Angle}}(\theta) = k_\theta(\theta - \theta_0)^2, \tag{3}$$

where $\theta_0 = 180^\circ$ and chose $k_\theta = 0$, 20, 70, and $100\,\varepsilon/\mathrm{rad}^2$ based on the Flory characteristic ratio C_∞, which has larger values as the polymer chain becomes stiffer. The values of C_∞ corresponding to k_θ are numerically calculated using $C_\infty = (1 + \langle\cos\theta\rangle)/(1 - \langle\cos\theta\rangle)$ [32]. The k_θ values correspond to $C_\infty = 1.75$, 80.34, 280.36, and 400.33, respectively. Interaction parameters and bead diameters for WCA potential [34] are set to $\varepsilon_{\mathrm{AA}} = \varepsilon_{\mathrm{BB}} = \varepsilon$ and $\sigma_{\mathrm{AA}} = \sigma_{\mathrm{BB}} = \sigma_{\mathrm{AB}} = \sigma$ respectively. To implement the excessive energy between different types of beads, we introduced $\tilde{\varepsilon} = \varepsilon_{\mathrm{AB}} - 0.5(\varepsilon_{\mathrm{AA}} + \varepsilon_{\mathrm{BB}})$, which is similar to the Flory–Huggins parameter χ, to describe the strength of incompatibility between the A and B beads [24,26]. We choose $\tilde{\varepsilon} = 9\varepsilon$ to simulate a strongly segregated system. The fundamental unit of time is $\tau = \sigma(m/\sigma)^{1/2}$, where m is the mass of a bead. All quantities are expressed by a combination of m, σ, and ε. All simulations are performed using the large-scale atomic/molecular massive parallel simulator (LAMMPS) molecular dynamics package [35].

The initial configuration of a homopolymer blends is constructed by attaching two different types of monodispersed homopolymer melts with unfavorable excess energy $\tilde{\varepsilon} = 9\varepsilon$. The monodisperse homopolymer melts, which are composed of M_{homo} chains consisting of N_{homo} beads, are obtained by using the method suggested by Auhl *et al.* [32]. The N_{homo} is set to 30 with $N_{\mathrm{homo,\,A}} = N_{\mathrm{homo,\,B}} = N_{\mathrm{homo}}$ and $M_{\mathrm{homo}} = 355$, thus the system contains $M_{\mathrm{homo}} \times (N_{\mathrm{homo,\,A}} + N_{\mathrm{homo,\,B}}) = 355 \times (30 + 30) = 21300$ beads. After the initial configuration is obtained, copolymers are inserted into the interface of the homopolymer blend. The number of copolymers at the interface M_{co} is increased in steps of 3 from 0 to 105 with simultaneous removal of homopolymers, which are arbitrarily chosen, with $M_{\mathrm{homo}} = 355 - (2/3)M_{\mathrm{co}}$, where $M_{\mathrm{homo}} = M_{\mathrm{homo,A}} = M_{\mathrm{homo,B}}$ to maintain the total number of beads. After the initial configurations of the homopolymer blend with a different number of copolymers are obtained, the $NPAT$ simulations which are suitable to evaluate interfacial tension $\gamma = f(P,T)$ with consideration of the anisotropy of the interfacial system [28] are performed, where N is the total number of beads, P is the pressure, A is the interfacial area, and T is the temperature of the system. Periodic boundary condition to all three directions is applied. In this particular system, we fixed the dimension of the x and y directions ($A_{xy} = L_x \times L_y = 23.3\sigma \times 23.3\sigma$) and the pressure in the z direction to $P_z = 5\varepsilon\sigma^{-3}$ with variable box length L_z to adjust the number density ρ to be near $0.85\sigma^{-3}$, which is the melt condition of the polymer simulation [24–27] by applying Berendsen barostat [36]. The temperature was kept at $T = 1.0\varepsilon/k_B$ using a Langevin thermostat with a frictional coefficient $\Gamma = 0.5\tau^{-1}$ [25,33]. The simulations were performed for $5 \times 10^6 \Delta t$ with time step $\Delta t = 0.01\tau$ to equilibrate the systems. The momentum drift of the system arising from random perturbations due to the Langevin thermostat is removed every $10\Delta t$. After equilibration runs, production runs are carried out for $\tau_T = 2.5 \times 10^7 \Delta t$ with the $NPAT$ ensemble to collect data for calculating the resulting properties.

III. RESULTS AND DISCUSSION

The density distributions ρ of the A/B homopolymer and AB copolymer system are analyzed, and the results are shown in Fig. 2. Figures 2(a)–2(f) show the density distributions when diblock (A-b-B) and grafted (A-g-B) copolymers are used as the compatibilizers with $M_{\mathrm{co}} = 63$, respectively, where M_{co} is the number of copolymers. The diblock copolymers with broad-shaped $\rho_{\text{A-b-B}}$ are more permeated into homopolymer melts than grafted copolymers, whereas grafted copolymers with narrow-shaped $\rho_{\text{A-g-B}}$ are more compactly located at the A/B interface. The conspicuous shape difference of the density

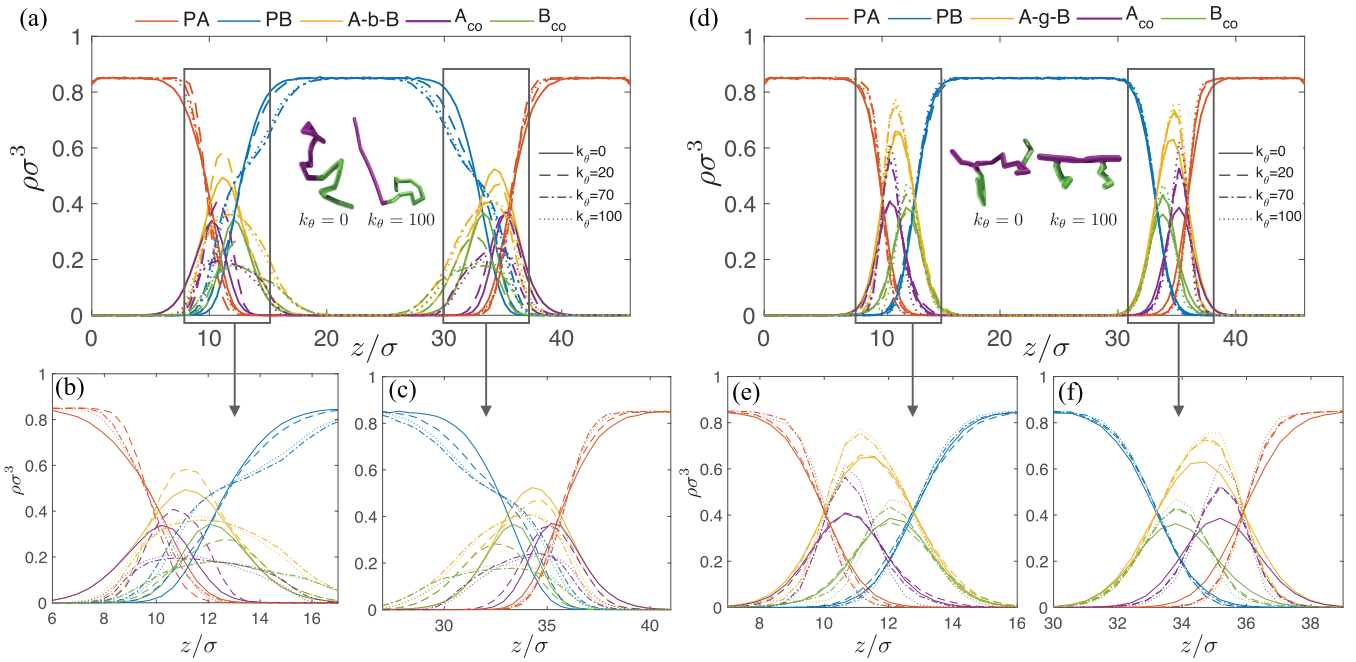

FIG. 2. Density distribution normal to the A/B interface (a–c) when diblock copolymers (A-b-B) and (d–f) two-arm grafted copolymers (A-g-B) are used as compatibilizer. The PA, PB, A_{co}, and B_{co} in the legend represent A homopolymer, B homopolymer, A block of copolymers, and B block of copolymers, respectively. Snapshots of diblock and grafted copolymers with different stiffness are given in insets of (a) and (d), respectively. The number of copolymers M_{co} is 63 in both cases.

distribution of diblock and grafted copolymers is due to the difference in copolymer structures. This trend becomes more obvious with an increase in the stiffness of the stiff subchain block consisting of A beads (SubA) controlled by k_θ. An increase in k_θ leads to the diblock copolymers pervading the B-rich phase more, while it leads to the grafted copolymers to be located more compactly at the interface as shown in Figs. 2(a) and 2(d).

To analyze the system more quantitatively, we calculated shape factor q of copolymers [14] defined as the relative difference of the squared radius of gyration between normal $R^2_{g,N} = R^2_{g,z}$ and parallel $R^2_{g,L} = 1/2(R^2_{g,x} + R^2_{g,y})$ to the

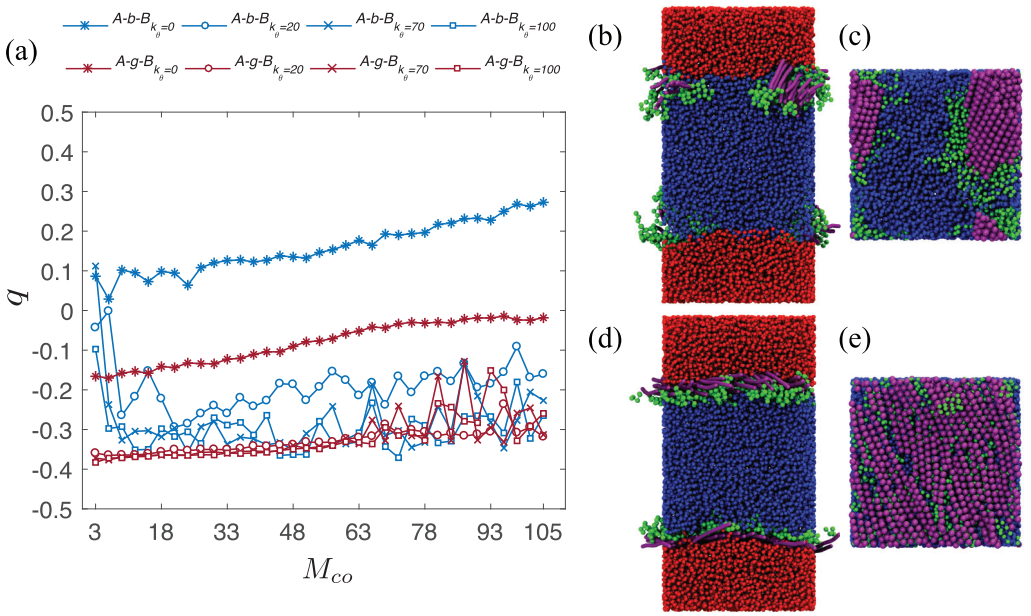

FIG. 3. (a) Shape factor q of copolymers defined as the relative difference of squared radius of gyration between normal $R^2_{g,N}$ and parallel $R^2_{g,L}$ to the interface. The snapshots of parallel (b) and normal (c) to the interface of diblock copolymers which form bundles at the interface. The snapshots of parallel (d) and normal (e) to the interface of grafted copolymers which cover the interface homogeneously. Simulation condition ($M_{co} = 63$, $k_\theta = 100\varepsilon/\text{rad}^2$) is applied for both diblock and grafted copolymers for the snapshots.

interface, i.e., $q = (R^2_{g,N} - R^2_{g,L})/R^2_g$ in Fig. 3(a). By definition, the value of q is in the range of $[-0.5, 1]$, physically representing [completely parallel to the interface, completely perpendicular to the interface]. As shown in Fig. 3(a), both diblock and grafted copolymers with $k_\theta = 0$ are stretched out toward A/B homopolymer region in the perpendicular direction to the A/B interface according to the increase in the number of copolymers $M_{\rm co}$. The ratio of $R^2_{g,N}$ to $R^2_{g,L}$, i.e., $\alpha = R^2_{g,N}/R^2_{g,L} = -(2q+1)/(q-1)$, is varied from 0.56 to 0.96 in the case of grafted copolymers, whereas it is varied from 1.09 to 2.12 in the case of diblock copolymers. Therefore, we can conclude that when copolymers are flexible with $k_\theta = 0$, diblock copolymers show deeper penetration into homopolymer regions compared to grafted copolymers.

Diblock copolymers with stiff SubA blocks tend to form bundles like a liquid-crystal [37,38] phase near the interface with increasing $M_{\rm co}$ due to the relatively favorable interaction between the SubA blocks of diblock copolymers arising from rigidity and anisotropic shape of SubA blocks [29–31,39]. The stiff SubA bundles make it difficult for the diblock copolymers to penetrate into A homopolymer region since stiff bundles significantly decrease the conformation entropy of A homopolymers by confining A homopolymers to a certain anisotropic structure formed by stiff bundles [9,29,40,41]. Therefore, when $M_{\rm co}$ is less than 6, where density of diblock copolymers is not enough to form a bundle structure, q parameter stays near 0 due to the relative free motion of diblock copolymers. However, when $M_{\rm co}$ is further increased, diblock copolymers tend to form bundles aligned in parallel to the interface which results in significant reduction of q parameter of diblock copolymers as shown in Figs. 3(a) and 3(b). To further examine the role of conformation entropy of homopolymers, we simulated diblock copolymers ($M_{\rm co} = 63$, $k_\theta = 100\varepsilon/\text{rad}^2$), while systematically changing the lengths of homopolymers $N_{\rm homo}$ from 1 to 30 in Fig. 4. At low $N_{\rm homo}$, conformation entropy loss of A homopolymers is small enough for penetration of the diblock copolymers bundles into the A homopolymer region. However, for longer chain of A homopolymer, significant loss of conformation entropy of A homopolymer prevents stiff bundles from penetrating into A homopolymer region which results in decreased q value. In addition, the pervasion of diblock copolymers into B homopolymer region is preferred than into A homopolymer region as shown in Figs. 2(a)–2(c) due to the maximized conformation entropy of B homopolymers at the interface by interacting with B block of diblock copolymers. Besides, the bundle formation of diblock copolymers causes the copolymers to partially cover the interface in an inhomogeneous fashion, which results in the direct contact of A/B homopolymer melts.

However, in the case of grafted copolymers with stiff SubA, the interface would be homogeneously covered by the aligned grafted copolymers because the branched chains grafted on the stiff backbone chain interfere with the bundle formation process. The homogeneous interfacial coverage of grafted copolymers prevents the direct contact of A homopolymers and B homopolymers. Most grafted copolymers with stiff SubA are stretched out in the parallel direction to the interface as shown in Figs. 3(a) and 3(c) and the shape factor q of grafted copolymers with stiff SubA fluctuates due to the spatial

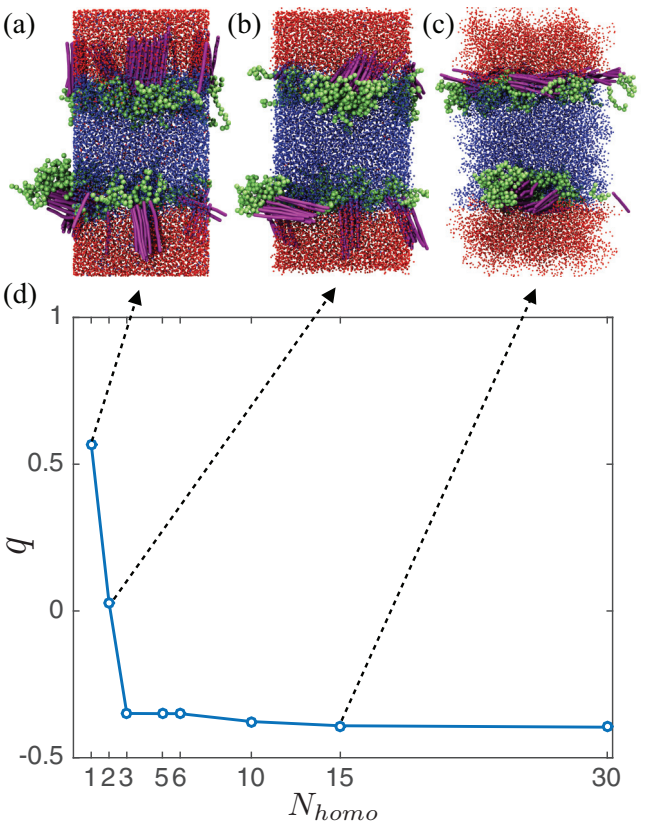

FIG. 4. The snapshots for the case of $N_{\rm homo} =$ (a) 1, (b) 2, and (c) 15 are also shown. (d) The shape factor q of diblock copolymer with ($M_{\rm co} = 63$, $k_\theta = 100\varepsilon/\text{rad}^2$) as a function of chain length $N_{\rm homo}$ of the A and B homopolymers.

constraint caused by the saturated interface when $M_{\rm co}$ is greater than or equal to approximately 63.

For the direct investigation of correlation between A and B homopolymers with interfacial properties, we calculated the pair distribution functions near the interface of A and B type beads in the homopolymers $g_{\rm AB}(r)$, which represents the probability of finding a B type bead at a distance of r away from an A type bead in Fig. 5. By comparing the solid lines

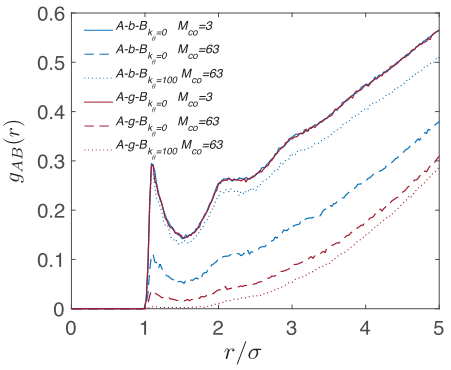

FIG. 5. The pair distribution function for A and B types of bead, $g_{\rm AB}(r)$, which represents the probability of finding B type of bead at a distance of r away from A type of bead.

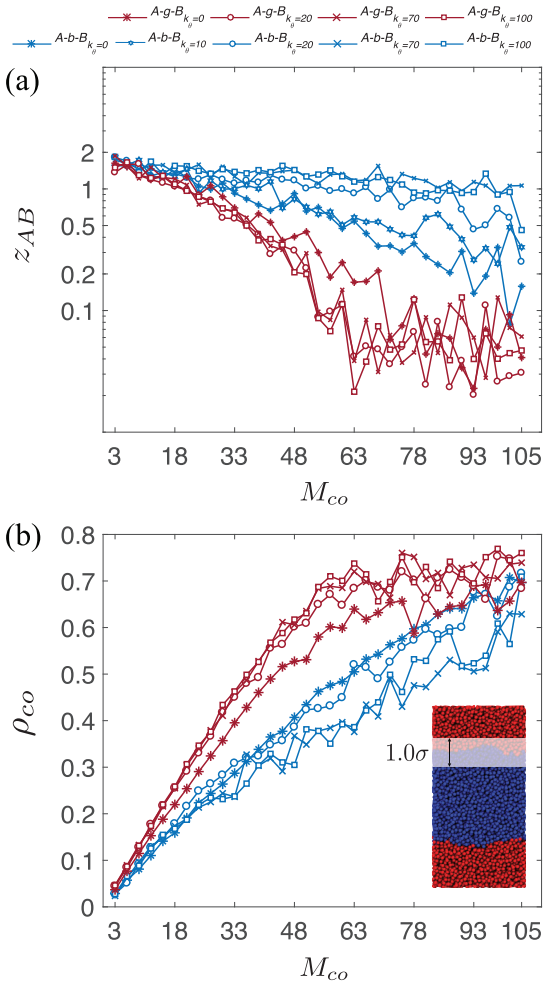

FIG. 6. (a) The coordination number z_{AB} between A and B beads defined as the integral of $g_{AB}(r)$ from 0 to the first minimum m_1, $z_{AB} = \int_0^{m_1} 4\pi r^2 \rho g_{AB}(r) dr$. (b) The number density of beads of copolymer ρ_{co} situated in the range from $z_0 - 0.5\sigma$ to $z_0 + 0.5\sigma$, where z_0 is the center of the interface.

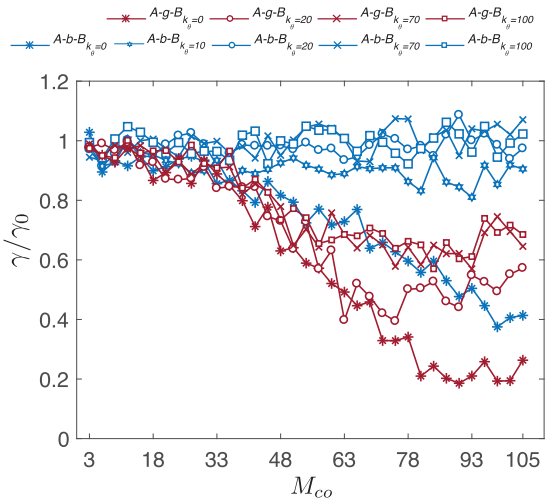

FIG. 7. Ratio of interfacial tension with copolymers to the interfacial tension without any copolymers γ/γ_0, where $\gamma_0 = 0.69 \pm 0.04\ \varepsilon\sigma^{-2}$, is shown. The interfacial tension γ is calculated using $\gamma = 1/2\langle L_z(P_N - P_T)\rangle$, where P_N and P_T are the pressure normal and tangential to the interface, respectively.

($M_{co} = 3$ and $k_\theta = 0\varepsilon/\text{rad}^2$) with the dashed lines ($M_{co} = 63$ and $k_\theta = 0\varepsilon/\text{rad}^2$) for both diblock and grafted copolymer cases in Fig. 5, it is clear that $g_{AB}(r)$ is decreased with increased M_{co} and the amount of decrease of $g_{AB}(r)$ is greater for grafted copolymers compared to that of diblock copolymers. This implies that the probability of direct interaction between A and B beads is significantly decreased with grafted copolymers. Furthermore, the increase in k_θ of diblock copolymers shows higher $g_{AB}(r)$, whereas that of grafted copolymers slightly decreases $g_{AB}(r)$ at the fixed M_{co} values. This is because the bundle formation between stiff SubAs of diblock copolymers induces the inhomogeneity of interfacial coverage and makes the A and B types of beads directly contact each other as shown in Fig. 3(b).

To quantitatively examine how well copolymers prevent the direct contact between A and B beads in different conditions, we evaluated the coordination number z_{AB} defined as the integral of $g_{AB}(r)$ from 0 to the first minimum m_1, $z_{AB} = \int_0^{m_1} 4\pi r^2 \rho g_{AB}(r) dr$. As shown in Fig. 6(a), the grafted copolymers lower the value of z_{AB} more effectively than diblock copolymers with increased M_{co}. To analyze this behavior, we calculated the number density of beads ρ_{co} of diblock and grafted copolymers in the range from $z_0 - 0.5\sigma$ to $z_0 + 0.5\sigma$, which is on the same order of unit length σ, where z_0 is the center of the interface. The ρ_{co} of grafted copolymers is always higher than that of diblock copolymers until the interface is saturated with grafted copolymers at approximately $M_{co} = 63$ or more as shown in Fig. 6(b). The result of ρ_{co} is also consistent with Figs. 2(a) and 2(d) and homogenous distribution of grafted copolymers compared to the inhomogeneous distribution of diblock copolymers at the interface.

For the direct comparison of the compatibilization efficiency, the interfacial tension γ defined as in Refs. [28,42–44] is calculated, where $P_N = P_{zz}$ and $P_T = 1/2(P_{xx} + P_{yy})$ are the pressure normal and tangential to the $\gamma = 1/2\langle L_z(P_N - P_T)\rangle$ interface, respectively. The angular bracket denotes the average over total time step τ_T and the pressure tensor is calculated by using the form of the virial tensor, $P_{lm} = 1/\tau_T \sum_{i=1}^{\tau_T} (1/V)[\sum_\alpha m^\alpha v_{i,l}^\alpha v_{i,m}^\alpha + r_{i,j}^\alpha f_{i,m}^\alpha]$, where m^α, $r_{i,l}^\alpha$, $v_{i,l}^\alpha$, and $f_{i,l}^\alpha$ are the mass, position, velocity, and total force acting on particle α at the ith time step for the l components (where l and $m = x, y, z$) [45]. Figure 7 shows the interfacial tension expressed as the ratio γ/γ_0, where $\gamma_0 = 0.69 \pm 0.04\ \varepsilon\sigma^{-2}$ is the precalculated interfacial tension without any copolymers. The amount of reduction of interfacial tension is bigger when using grafted copolymers compared to diblock copolymers as a compatibilizer with increase in M_{co}. Relatively high γ values of diblock copolymers with $k_\theta \neq 0$ can be explained by increased probability of direct contact of A and B homopolymers due to the inhomogeneous interfacial coverage of stiff diblock copolymers. The results are consistent with that of previous studies in that γ is increased with stiff surfactantlike molecules due to an increase in the absolute amount of surface free energy induced by the bending potential [44,46,47] and the entropic contribution to excess free energy arising from stiffness disparities [48–50]. It is noted that the

trend of the interfacial tension γ is analogous to the results of z_{AB} given in Fig. 6(a), which is reasonable since z_{AB} represents the average number of direct contacts between A and B beads.

IV. CONCLUSION

We studied the effects of the structures of the copolymers (diblock and grafted copolymers) and the stiffness of one of the blocks of copolymers on the interfacial properties of an immiscible polymer blend. It is examined that an asymmetric increase in the stiffness of diblock copolymers causes anomalous behaviors, making it a poor compatibilizer. The inhomogeneous interfacial coverage results in direct contact of two homopolymer regions, which have thermodynamically unfavorable interaction. The orientational constraint resulting from balancing conformational entropies between A homopolymer and stiff SubA bundles makes SubA bundles pervade into B homopolymer region. However, stiffer SubA chain of grafted copolymers are located more compactly at the interface of two homopolymers and cover the interface more homogenously by hindering bundle formation due to the branched chains. Finally, we calculated the interfacial tension for the direct comparison of compatibilizer efficiency of diblock and grafted copolymers. As a result, interfacial tension is efficiently reduced by using grafted copolymers as compatibilizers compared to block copolymers for all stiffness conditions for relatively short copolymer chain length. Our results suggest a better molecular design strategy of compatibilizers for polymer blend systems for numerous future applications.

ACKNOWLEDGMENTS

This work was supported by the National Institute of Supercomputing and Network, Korea Institute of Science and Technology Information, with supercomputing resources including technical support KSC-2015-C2-034, and the National Research Foundation of Korea (Grant No. 2015R1A2A2A01007379). The authors declare no competing financial interest.

[1] H. J. Kim, J. H. Kim, J. H. Ryu, Y. Kim, H. Kang, W. B. Lee, T. S. Kim, and B. J. Kim, Acs Nano **8**, 10461 (2014).
[2] G. Li, V. Shrotriya, J. S. Huang, Y. Yao, T. Moriarty, K. Emery, and Y. Yang, Nat. Mater. **4**, 864 (2005).
[3] G. Yu, J. Gao, J. C. Hummelen, F. Wudl, and A. J. Heeger, Science **270**, 1789 (1995).
[4] D. Kipp, R. Verduzco, and V. Ganesan, J. Polym. Sci. Pol. Phys. **54**, 884 (2016).
[5] D. Kipp, J. Mok, J. Strzalka, S. B. Darling, V. Ganesan, and R. Verduzco, Acs Macro Lett. **4**, 867 (2015).
[6] B. A. Ibrahim and K. M.Kadum, Mod. Appl. Sci. **4**, 157 (2010).
[7] B. J. Kim, H. M. Kang, K. Char, K. Katsov, G. H. Fredrickson, and E. J. Kramer, Macromolecules **38**, 6106 (2005).
[8] K. Binder, M. Muller, F. Schmid, and A. Werner, Physica A **249**, 293 (1998).
[9] G. Fredrickson, *The Equilibrium Theory of Inhomogeneous Polymers* (Oxford University Press, Oxford, 2013).
[10] F. S. Bates, Science **251**, 898 (1991).
[11] M. W. Matsen and F. S. Bates, Macromolecules **29**, 1091 (1996).
[12] Y. Lyatskaya and A. C. Balazs, Macromolecules **29**, 7581 (1996).
[13] S. H. Anastasiadis, I. Gancarz, and J. T. Koberstein, Macromolecules **22**, 1449 (1989).
[14] A. Werner, F. Schmid, K. Binder, and M. Muller, Macromolecules **29**, 8241 (1996).
[15] A. Werner, F. Schmid, and M. Muller, J. Chem. Phys. **110**, 5370 (1999).
[16] Y. Lyatskaya, D. Gersappe, N. A. Gross, and A. C. Balazs, J. Phys. Chem.-Us **100**, 1449 (1996).
[17] Y. Lyatskaya, D. Gersappe, and A. C. Balazs, Macromolecules **28**, 6278 (1995).
[18] A. Faldi, J. Genzer, R. J. Composto, and W. D. Dozier, Phys. Rev. Lett. **74**, 3388 (1995).
[19] R. A. Riggleman, R. Kumar, and G. H. Fredrickson, J. Chem. Phys. **136**, 024903 (2012).
[20] S. M. Hur, C. J. Garcia-Cervera, E. J. Kramer, and G. H. Fredrickson, Macromolecules **42**, 5861 (2009).
[21] V. Mishra, S. M. Hur, E. W. Cochran, G. E. Stein, G. H. Fredrickson, and E. J. Kramer, Macromolecules **43**, 1942 (2010).
[22] J. U. Kim, Y. B. Yang, and W. B. Lee, Macromolecules **45**, 3263 (2012).
[23] A. Facchetti, Chem. Mater. **23**, 733 (2011).
[24] G. S. Grest, M. D. Lacasse, K. Kremer, and A. M. Gupta, J. Chem. Phys. **105**, 10583 (1996).
[25] K. Kremer and G. S. Grest, J. Chem. Phys. **92**, 5057 (1990).
[26] M. Murat, G. S. Grest, and K. Kremer, Macromolecules **32**, 595 (1999).
[27] J. H. Ryu, H. S. Wee, and W. B. Lee, Phys. Rev. E **94**, 032501 (2016).
[28] Y. Zhang, S. E. Feller, B. R. Brooks, and R. W. Pastor, J. Chem. Phys. **103**, 10252 (1995).
[29] M. Doi and S. F. Edwards, *The Theory of Polymer Dynamics* (Clarendon Press, Oxford, UK, 1988).
[30] M. Lee, B. K. Cho, and W. C. Zin, Chem. Rev. **101**, 3869 (2001).
[31] Y. Li, T. Jiang, S. Lin, J. Lin, C. Cai, and X. Zhu, Sci. Rep. **5**, 10137 (2015).
[32] R. Auhl, R. Everaers, G. S. Grest, K. Kremer, and S. J. Plimpton, J. Chem. Phys. **119**, 12718 (2003).
[33] G. S. Grest and K. Kremer, Phys. Rev. A **33**, 3628 (1986).
[34] J. D. Weeks, D. Chandler, and H. C. Andersen, J. Chem. Phys. **54**, 5237 (1971).
[35] S. Plimpton, J. Comput. Phys. **117**, 1 (1995).
[36] H. J. C. Berendsen, J. P. M. Postma, W. F. Vangunsteren, A. Dinola, and J. R. Haak, J. Chem. Phys. **81**, 3684 (1984).
[37] M. W. Matsen and C. Barrett, J. Chem. Phys. **109**, 4108 (1998).
[38] R. Mezzenga, W. B. Lee, and G. H. Fredrickson, Trends Food Sci. Tech. **17**, 220 (2006).
[39] M. H. M. Cativo *et al.*, Acs Nano **8**, 12755 (2014).
[40] Y. Kim, E. Ha, and A. Alexander-Katz, Macromolecules **44**, 7016 (2011).
[41] F. S. Bates and G. H. Fredrickson, Phys. Today **52**, 32 (1999).
[42] J. G. Kirkwood and F. P. Buff, J. Chem. Phys. **17**, 338 (1949).
[43] E. Helfand and Y. Tagami, J. Chem. Phys. **57**, 1812 (1972).

[44] R. Goetz and R. Lipowsky, J. Chem. Phys. **108**, 7397 (1998).
[45] W. B. Lee and K. Kremer, Macromolecules **42**, 6270 (2009).
[46] Y. Zhou, X. P. Long, and Q. X. Zeng, Polymer **52**, 6110 (2011).
[47] A. Milchev, J. Chem. Phys. **143**, 064701 (2015).
[48] G. H. Fredrickson, A. J. Liu, and F. S. Bates, Macromolecules **27**, 2503 (1994).
[49] C. Singh and K. S. Schweizer, J. Chem. Phys. **103**, 5814 (1995).
[50] C. Singh and K. S. Schweizer, Macromolecules **30**, 1490 (1997).